ANALYSIS ON FAULT TRANSMISSION CHARACTERISTICS OF TOOTH ROOT CRACK IN FIXED AXIS GEAR

Xin WANG[1], Weiliang ZHANG[2*], Xiaofei ZHAO[3,4], Liang LI[5]

Wind turbine gear transmission system test rig is taken as the research object. The three-dimensional solid rigid-flexible coupling model is established. Through dynamic simulation, contact force signals of each gear pair are obtained under fixed axis gear tooth root crack state. The transmission characteristics of system are analyzed under normal and crack fault state. According to the component composition, amplitude change and contribution size of each transfer path. The correlation between the paths and transmission characteristics of crack faults were obtained in transmission process of gear contact force signals to response points on the surface of gearbox.

Keywords: multistage gear transmission system, rigid-flexible coupling model, crack, transfer characteristic, correlation

1. Introduction

Crack is a common fault of gear transmission system. At present, fault model of cracked gear and analysis results are not accurate enough, and further study is needed.

In recent years, some scholars have studied the mode shapes, natural frequencies and meshing stiffness of cracks by finite element simulation [1-2]. But the mechanism of crack fault needs further study. The fault diagnosis technology of gear box cannot solve the problem of crack fault identification in multi-gear transmission system. According to the actual movement rule of the system, it is particularly important to propose a targeted fault identification method.

Some scholars built dynamic models and solved the dynamic response signal of fault gear teeth, to analyze the corresponding spectrum characteristics.

[1] Dr., School of Mechanical Engineering, Baoji University of Arts and Sciences, Baoji, 721016, China, e-mail: 46607190@qq.com
[2] School of Mechanical Engineering, Baoji University of Arts and Sciences, Baoji, 721016, China, e-mail: zhangweiliang-243@163.com
[3] Eng., School of Mechanical Engineering , Tianjin Polytechnic University, Tianjin, 300387, China, e-mail: 604526055@qq.com
[4] Eng., Bethel Automotive Safety Systems Co., Ltd, Anhui, 241000, China, e-mail: 604526055@qq.com
[5] School of Mechanical Engineering, Baoji University of Arts and Sciences, Baoji, 721016, China, e-mail: 18468564@qq.com

Chen [3] built a planetary gear train dynamics model considering meshing rigidity and other factors. He solved and analyzed the vibration characteristics and side band characteristics of the internal gear ring with gear root crack fault. Liang [4] analyzed and evaluated the effect of cracks on the meshing stiffness of planetary gears by establishing a tooth crack model. However, it is different from the response signals detected on the surface of gear box in actual fault diagnosis.

It is also a mainstream method to separate and extract fault signals directly from gear box surface by using advanced algorithm. Liu [5] proposed a novel wind turbine fault diagnosis method based on the local mean decomposition (LMD) technology, and successfully extracted the frequency characteristics of local crack faults of wind turbine planetary gearbox gears. Li [6-7] used the combined intelligent signal analysis method based on wavelet packet, empirical mode decomposition, wigner distribution and AR model to identify five single faults and three coupling faults. Then he proposed a new method [8], using the independent component analysis (ICA - R) as the fault frequency tracking tool to simplify the coupling fault to a single fault. Luo [9] proposed a sparse representation method based on wavelet basis for compound fault feature extraction, which can separate and extract different transient characteristics of bearings and gears. However, when using the surface signal of gear box to identify the fault, different measuring points also have great influence on the result. When the vibration signal is transmitted from the inside of the gear box to the surface of the gear box, it will change in different paths [10]. Therefore, attention should be paid to the study of the transmission characteristics of the gearbox signal.

Liu [11] proposed a comprehensive vibration signal model for a planetary gear set considering all the vibration sources and transmission path effects. At present, most of the researches on transmission characteristics of gear boxes focus on the single-stage planetary gear boxes or the fixed axis gear boxes. Multilevel meshing and multiple transmission paths will interact with each other for wind turbine gearboxes which including two-stage fixed-axis gears and one-stage planetary gear train. When a fault occurs in one stage of meshing, it will appear in the form of other meshing frequencies in the power spectrum [12-13]. Therefore, the fault characteristics and fault transmission characteristics of wind turbine gear system should be studied specifically.

2. Dynamic model of wind turbine gear transmission system

2.1 Fault simulation test rig for wind turbine gear box

The wind turbine gearbox fault simulation test rig, shown in Fig. 1, is taken as the research object. Fault transmission characteristic analysis and fault diagnosis of multistage gearbox are carried out.

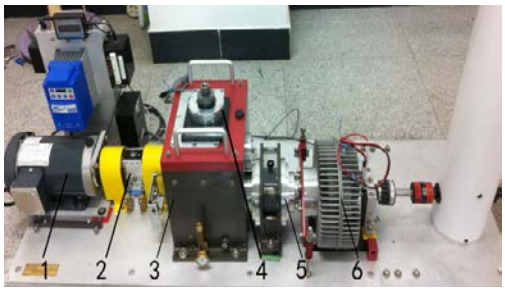

Fig. 1. The test rig of gear transmission system: 1-Motor, 2-Torque sensor and encoder, 3-Two stage fixed-axis gearbox, 4-Radial load of bearing, 5-One stage planetary gearbox, 6-Brake

The gearbox system of the test rig is made up of two-stage fixed axis gears and one-stage planetary gear train, as shown in Fig. 2.

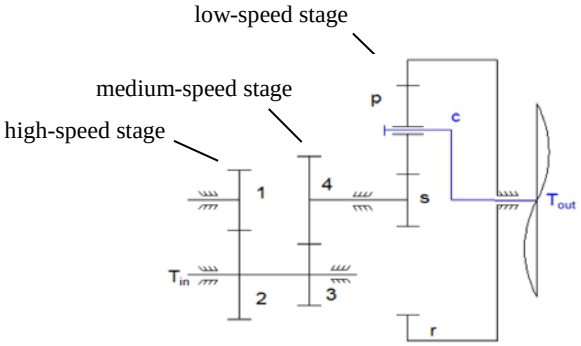

Fig. 2. Structure diagram of the gear transmission system test rig

where, T_{in} is the input torque, driven by three-phase AC asynchronous motor. T_{out} is the output torque, which can be set through the electromagnetic powder brake. Gears 1 and 2 form high-speed gear pair. Gears 1 and 2 are high-speed driven. Gears 3 and 4 are medium-speed driving gear and driven gear respectively. The planetary gear train is low-speed stage, p is planetary gear, s is sun gear, c is planet carrier, and r is ring gear (fixed). The gears in the test rig are involute cylindrical spur gears with pressure angle of 20° , material of S45C and density of 0.00785 g/mm^3. Gear parameters are shown in Table 1.

Table 1

Gear parameters

Gear	Number of teeth	R_{ri}/mm	R_{bi}/mm	Mass m_i/g	J_i/(g·m^2)	Face width /mm	Module/mm
1	29	19.2	20.4	125	0.05	30	1.5
2	100	68.9	70.5	1224.5	6	30	1.5
3	36	23.9	25.3	224	0.14	30	1.5
4	90	61.5	63.4	1111	4	20	1.5
s	28	12.3	13	41	0.007	20	1.0
pn	36	16	17	34.6	0.01	20	1.0
c			30	848.7	0.76	20	1.0
r	100	45.6	47			20	1.0

2.2 Transfer path and transfer function

The vibration transfer path system model of multistage gear transmission system is established by system identification method. The multi-degree-of-freedom vibration differential equation of the system is [14]

$$[M]\{\ddot{x}\}+([K]+j[\eta])\{x\}=\{f(t)\}. \tag{1}$$

The above formula can be rewritten as

$$[M]\{\ddot{x}\}+[K_g]\{x\}=\{f(t)\}. \tag{2}$$

where, $[K_g]=[K]+j[\eta]$ is complex stiffness matrix, which considers structural damping as a form of stiffness effect.

The Laplace transform of equation (2) is

$$(s^2[M]+[K_g])\{X(s)\}=\{F(s)\}. \tag{3}$$

order

$$[Z(s)]=[M]s^2+[K_g]. \tag{4}$$

where, $[Z(s)]$ has the property of stiffness, which is called dynamic stiffness of system. Under a certain excitation, its value is inversely proportional to the system response $\{X(s)\}$. That is, it has the function of impedance system vibration. Therefore, $[Z(s)]$ is also called mechanical impedance of system. Its reciprocal is called transfer function, which is expressed in $[H(s)]$, that is,

$$[H(s)]=([M]s^2+[K_g])^{-1}. \tag{5}$$

By equation (3) there is

$$[H(s)]=\frac{\{X(s)\}}{\{F(s)\}}. \tag{6}$$

For a real vibration system, replacing s with $j\omega$ does not lose useful information. Therefore, the Fourier transform is performed on both sides of the equation (1) to get

$$\{X(\omega)\}=[H(\omega)]\{F(\omega)\}. \tag{7}$$

$$[H(\omega)]=\frac{\{X(\omega)\}}{\{F(\omega)\}}. \tag{8}$$

That is, the transfer function in Laplace domain $[H(s)]$ becomes the frequency response function in Fourier domain $[H(\omega)]$.

The frequency response function $H(\omega)$ can fully describes the dynamic characteristics of system. That is, system changes with frequency, stiffness and damping. Its physical meaning is: if a sine excitation is input at frequency ω, system will also produce a sinusoidal output response at ω [15]. Therefore, the vibration transfer relation of multistage gear system is expressed by frequency response function [16].

2.3 Dynamic model of gear box

Taking the wind turbine gearbox fault simulation test rig as prototype, the corresponding 3D solid model is established and imported into ADAMS for dynamic simulation. Considering nonlinear characteristics of gear box, the fixed axis gear box and the planetary gear box are softened [17-18] to obtain more real gear dynamics characteristics. The gear, axis, box and other components are built, and gearboxes are integrally assembled by applying constraint relations. The assembled body and its internal structure are shown in Fig. 3.

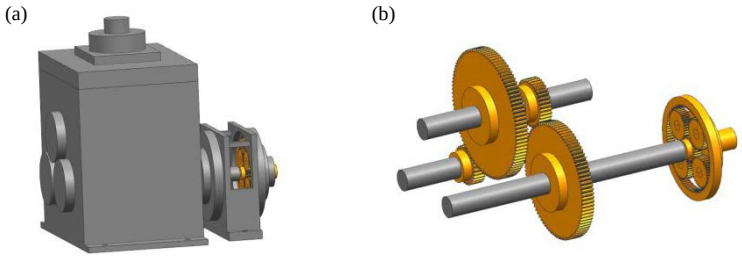

Fig. 3. Wind turbine gear box test rig solid model: (a) assembled body, and (b) internal structure

3. Analysis of dynamic excitation signal of gear meshing

The gear contact force can fully reflect dynamic response characteristics of gear meshing process, and contribute to the qualitative analysis of system dynamic characteristics and fault characteristics under fault state. Using the model in Fig. 3, dynamic simulation is set up and the dynamic equations of gearbox during running process are established. Solve the contact force signals under normal and high-speed driving gear (gear 1) with root crack fault states. A constant drive torque of 14400°/s (40Hz) is applied to the high-speed axis. A load torque of 300000 N/mm is applied to the planet carrier. Both the drive torque and the load torque reach the established values in form of STEP function within 0.01s, STEP (time, 0, 0, 0.01, 14400d) and STEP (time, 0, 0, 0.01, 300000). Characteristic frequency parameters of gears at all levels in the test rig are shown in Table 2.

Table 2

Main frequency parameters

Characteristic frequency	Value
High-speed meshing frequency f_1	1160 Hz
Medium-speed meshing frequency f_2	417.6 Hz
Low-speed (planetary) meshing frequency f_3	101.5 Hz
High-speed gear failure characteristic frequency f_d	40 Hz
Planetary failure characteristic frequency f_r	2.819Hz

3.1 Analysis of gear contact force signal under normal state

The dynamic simulation of system under normal state is carried out. The contact force simulation signals of high-speed, medium-speed and low-speed external meshing (planetary gear meshing with sun gear) and low-speed internal meshing (planetary gear meshing with ring gear) in gear box are respectively extracted, as shown in Fig. 4.

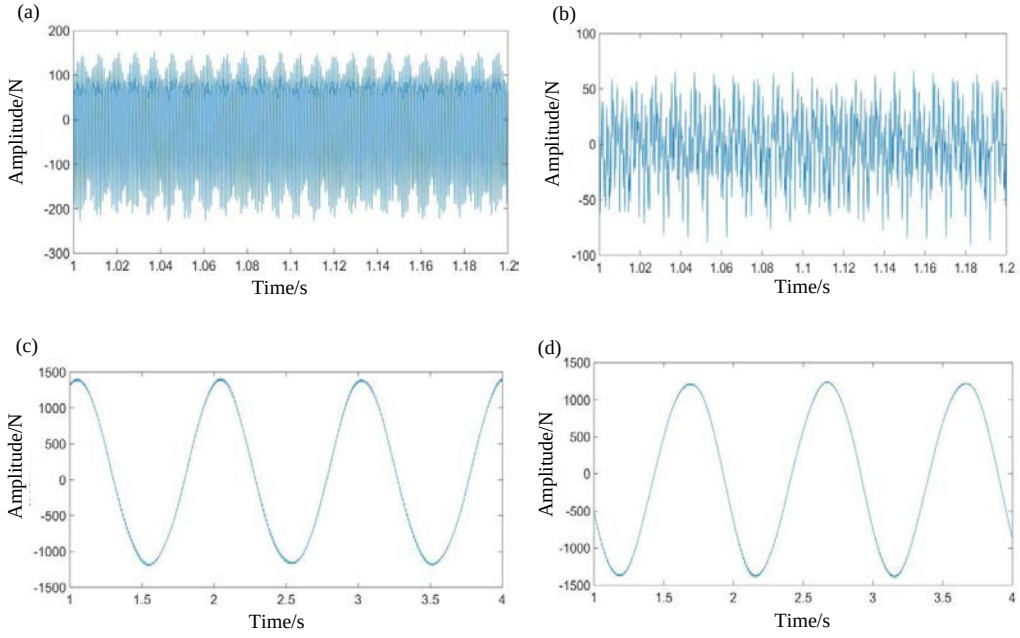

Fig. 4. Time domains of gear contact force simulation signal under normal state: (a) high-speed, (b) medium-speed, (c) low-speed external meshing, and (d) low-speed internal meshing

As can be seen from Figs. 4a and b, the waveforms of high-speed and medium-speed signals are relatively dense, mainly composed of high frequency component. In Figs. 4c and d, the amplitude of low-speed contact force signal is large. Since the positions of meshing points of low-speed external meshing and the low-speed internal meshing change with the rotation of planet carrier, the vibration transfer paths between meshing points and box is changed. The passing effect of planetary gear will cause the amplitude modulation of meshing vibration. The planet carrier rotation frequency is the modulation frequency.

In order to observe the frequency components and the proportion in signals, power spectrum corresponding to each time domain signal is obtained, as shown in Fig. 5.

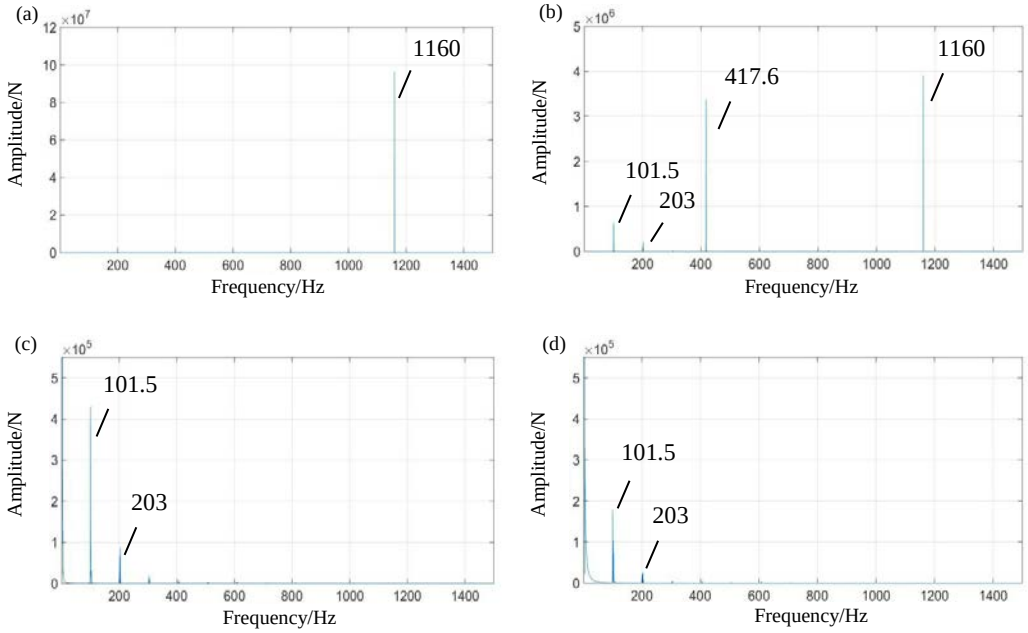

Fig. 5. Frequency domains of gear contact force simulation signal under normal state: (a) high-speed, (b) medium-speed, (c) low-speed external meshing, and (d) low-speed internal meshing

In high-speed signal (Fig. 5a), the vibration frequency is dominated by high-speed meshing frequency f_1 (1160 Hz). Medium-speed meshing frequency f_2 (417.6 Hz) and low-speed meshing frequency f_3 (101.5 Hz) are relatively weak and hardly visible.

In medium-speed signal (Fig. 5b), in addition to medium-speed meshing frequency f_2 (417.6Hz), there are also high-speed meshing frequency f_1 (1160Hz), low-speed meshing frequency f_3 (101.5Hz) and its doubled frequency $2f_3$ (203Hz). It shows the correlation between various gear signals.

In Figs. 5c and d, high-speed meshing frequency f_1 (1160Hz) and medium-speed meshing frequency f_2 (417.6Hz) attenuate obviously. The frequency components are mainly low-speed meshing frequency f_3 (101.5Hz) and its frequency multiplication ($2f_3$, $3f_3$...). The response frequency amplitude of low-speed external meshing (Fig. 5c) is larger than that of low-speed internal meshing (Fig. 5d).

The above time domain and frequency domain charts conform to the basic law and verify the correctness of model.

3.2 Analysis of gear contact force signal under the state of root crack fault of fixed axis gear

Set the high-speed driving gear (gear 1) to have a root crack fault. The crack depth is consistent with the crack gear in test rig, as shown in Fig. 6. Fig. 6a

shows the actual gear with root crack fault. Fig. 6b shows the corresponding simulation gear model with root crack fault.

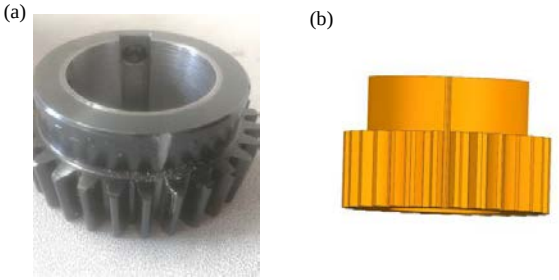

Fig. 6. Crack fault gear: (a) actual gear with root crack fault, (b) simulation gear model with root crack fault

It is found that the crack fault of high-speed gear has little influence on the vibration response of low-speed gear (planetary gear train), which mainly affects the high-speed and medium-speed gears. Only the time domain and frequency domain diagrams of contact force signals in high-speed and medium-speed fault states are listed, as shown in Fig. 7.

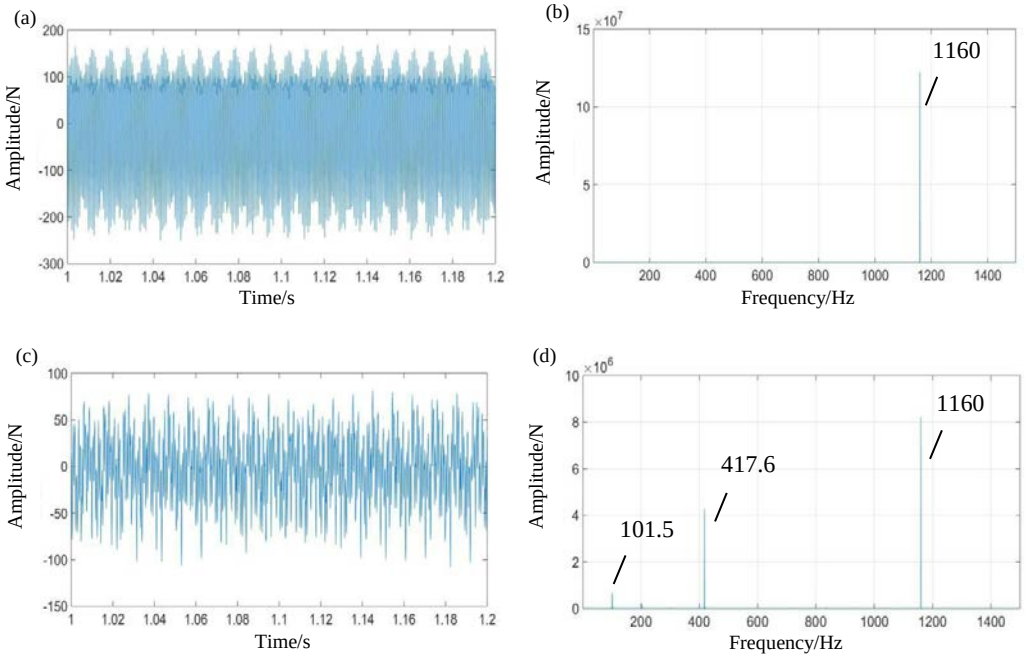

Fig. 7. Gear contact force simulation signal under the state of crack in the tooth root of high-speed driving gear: (a) high-speed time domain, (b) high-speed frequency domain, (c) medium-speed time domain, and (d) medium-speed frequency domain

Comparing Figs. 7a and 4a, the root crack as a weak fault [19-20] does not produce a significant periodic impulse for high-speed stage signal, but its vibration amplitude increases from -230N~+150N to -250N~+165N. Comparing

Figs. 7b and 5a, it can be seen that the crack fault increases the meshing frequency amplitude of high-speed gear from 9.6×10^7N to 1.3×10^8N. The increase is significant.

Comparing Figs. 7c and 4b, the vibration amplitude of medium-speed also increases. Comparing Figs. 7d and 5b, high-speed meshing frequency f_1 (1160 Hz), medium-speed meshing frequency f_2 (417.6 Hz) and its multiple frequency ($2f_2$, $3f_2$...) in power spectrum are all significantly increased on the amplitude. It is also confirmed that there is a mutual influence between high-speed and medium-speed vibration responses.

4. Test signal analysis and transfer function calculation of test rig

4.1 Test signal characteristics under normal state

The acceleration response signals on the surface of gearboxes under normal state were measured, in which the input axis frequency was 40Hz, the output axis was loaded with 10V, and the sensitivity of acceleration sensor was 100.2mv /g. Considering the difference of collected signals on different boxes, the acceleration vibration response signals of fixed-axis gearbox and planetary gearbox in horizontal direction were measured separately. The test results of two boxes on the surface under normal state are shown in Fig. 8.

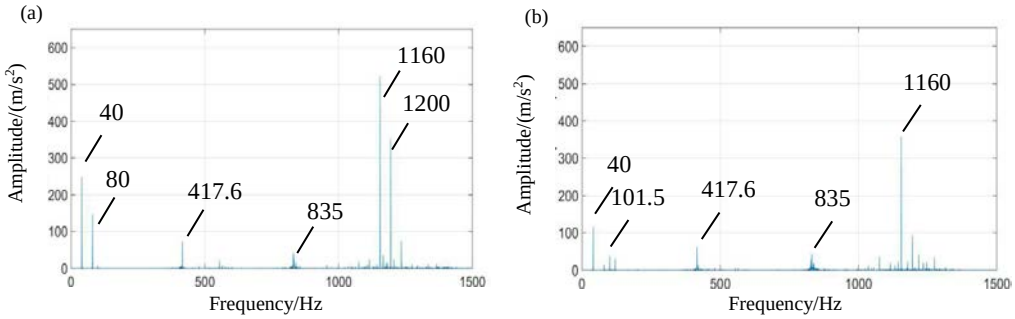

Fig. 8. Power spectrum signals of test rig under normal state: (a) fixed axis gear box, and (b) planetary gear box

It can be seen from Fig. 8 that the main frequency components of two boxes in normal state are high-speed meshing frequency f_1 (1160 Hz), high-speed axis frequency f_d (40 Hz), medium-speed meshing frequency f_2 (417.6 Hz) and its frequency doubling $2f_2$ (835Hz), low-speed meshing frequency f_3 (101.5Hz), etc.

Affected by distance, the signal intensities of two boxes is different. In Fig. 8b, input axis rotation frequency f_d (40Hz) and high-speed meshing frequency f_1 (1160Hz) are significantly weakened because of far away from high-speed stage. The amplitude of low-speed meshing frequency f_3 (101.5Hz) is enhanced.

4.2 Transfer function of each transfer path under normal state

Take the four contact forces in Fig. 5 as the input excitation forces and the test signals on the surface of gearbox in Fig. 8 as the output. The multi-point input single-point output model is used to solve the problem. The amplitude-frequency response curves of transfer functions of meshing excitation forces transmitted to fixed-axis gearbox and planetary gearbox under normal state are shown in Fig. 9.

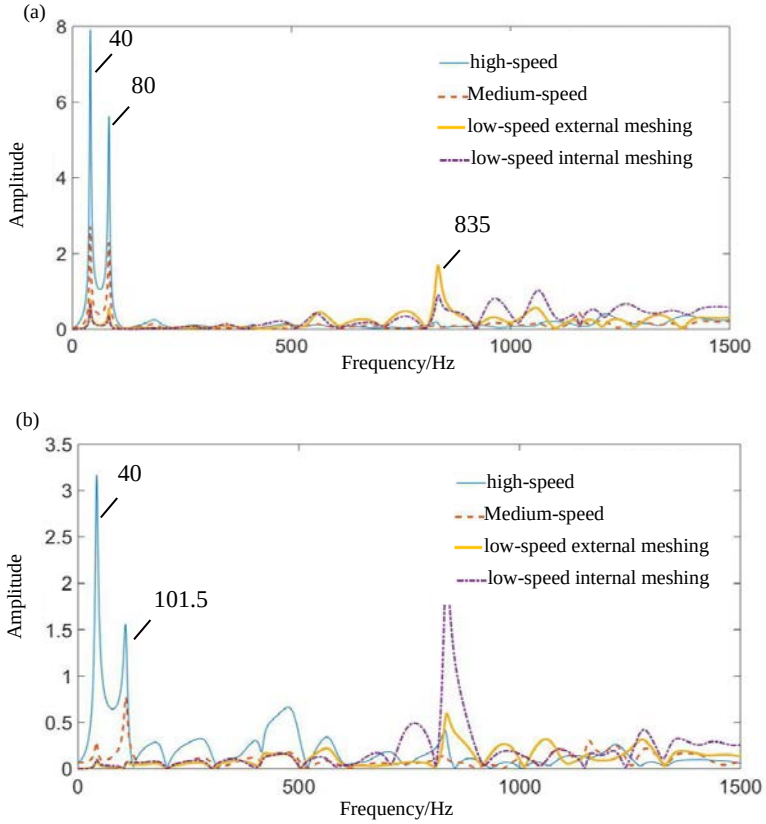

Fig. 9. The amplitude-frequency response curve of transfer function of each transfer path under normal state: (a) contact forces are transmitted to fixed axis gearbox, and (b) contact forces are transmitted to planetary gearbox

In Fig. 9a, 40Hz has the highest amplitude, and the frequency is high-speed axis frequency. Therefore, high-speed stage contact force has the greatest contribution to the frequency, and medium-speed and low-speed stage also have some contributions. Meshing frequencies of f_1, f_2 and f_3 are not obvious. But meshing frequency of $2f_2$ (835Hz) are obvious, which is the contribution of low-speed internal and external meshing process [21].

In Fig. 9b, planetary gearbox is far away from high-speed stage, signal intensity of high-speed stage is weakened, and low-speed signal is enhanced. The amplitude of high-speed axis rotation frequency f_d (40Hz) decreases. The

frequency characteristic of low-speed meshing frequency f_3 (101.5Hz) increases. Low-speed internal and external meshing also causes a large value of $2f_2$ (835 Hz).

4.3 Test signal characteristics of fixed-axis gear root crack

The normal high-speed driving gear was replaced with the fault gear in Fig. 6a. Test signals of two boxes are shown in Fig. 10.

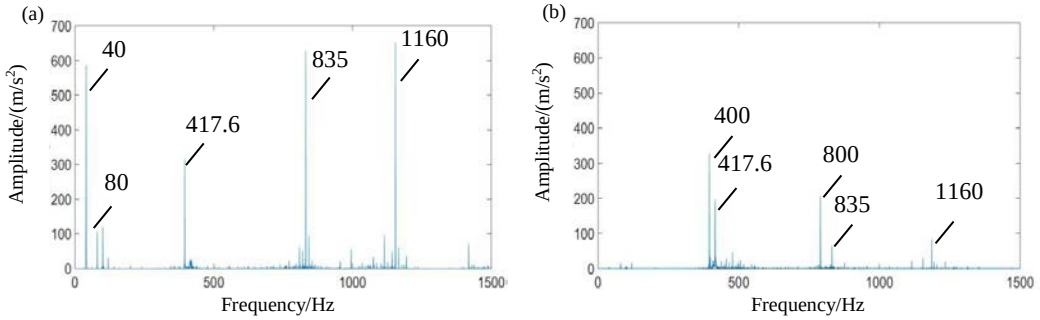

Fig. 10. Power spectrum signals of test rig under high-speed driving gear with tooth root crack: (a) fixed axis gear box, and (b) planetary gearbox

Compared with Figs. 10a and 8a, the amplitude of high-speed meshing frequency f_1 (1160Hz) and high-speed axis rotation frequency f_d (40Hz) rises as a result of high-speed fault. The amplitude of f_2 (417.6hz) and $2f_2$ (835Hz) increase significantly, which are the associated fault features caused by root crack of high-speed gear. The reason may be that the vibration caused by high-speed fault causes more load fluctuations at high-speed and aggravates the vibration of medium-speed gear.

In Fig. 10b, planetary gear box is far away from the fault gear, and high-speed meshing frequency f_1 (1160Hz) amplitude is not high. Since medium-speed gear is coaxial with sun gear, medium-speed vibration with obvious amplitude in Fig. 10a is transmitted to planetary gear box, which increases the amplitudes of medium-speed meshing frequency f_2 (417.6Hz) and its frequency doubling $2f_2$ (835Hz) in vibration signal of planetary gear box. There is a 400Hz frequency component near 417.6Hz with very high amplitude, which is 4 times meshing frequency of planetary gear $4f_3$ (400Hz). Due to proximity to 417.6 Hz, the two resonate. Similarly, 800 Hz appears near 835 Hz.

The above shows that the crack fault not only affects high-speed stage, but also affects other gears. In order to analyze the causes and components of these association fault frequencies, further exploration is needed through transmission characteristic analysis [22].

4.4 Transfer function of each transfer path under the state of fixed axis root crack

Take the four contact forces in Fig. 5 as the input excitation forces and the

test fault signals on the surface of gearbox in Fig. 10 as the output. The amplitude-frequency response curves of transfer functions of meshing excitation forces transmitted to fixed-axis gearbox and planetary gearbox under normal state are shown in Fig. 11.

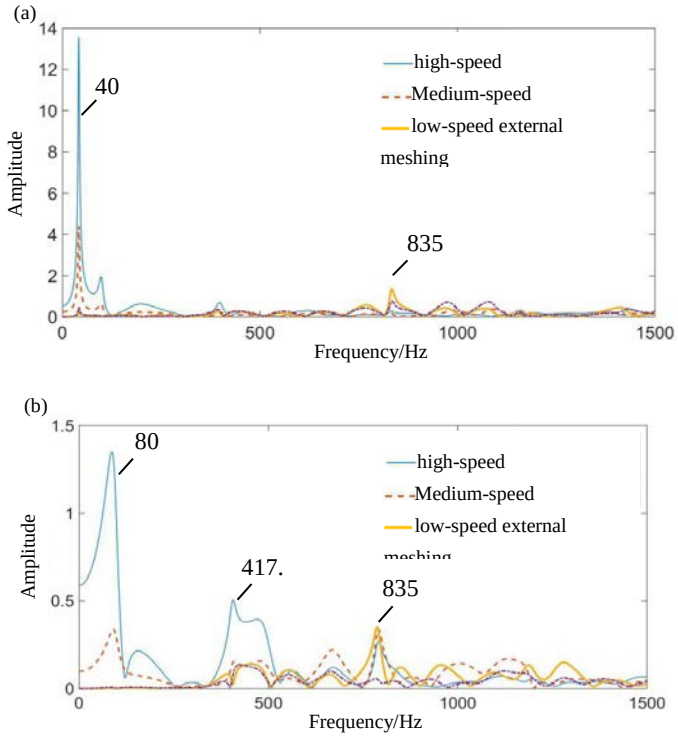

Fig. 11. The amplitude-frequency response curve of transfer function of each transfer path under high-speed driving gear tooth root crack: (a) contact forces are transmitted to the fixed axis gearbox, and (b) contact forces are transmitted to the planetary gearbox

As the amplitude of high-speed axis rotation frequency f_d (40Hz) in Fig.10a increases, so does the amplitude of f_d in Fig.11a. This is consistent with the fault characteristic of gear local fault. 835Hz is caused by low-speed internal and external meshing, which is the same as Fig. 9a, and this feature is not affected.

The main peak in Fig. 11b is 80Hz, which is the frequency doubling of high-speed axis rotation frequency f_d (40Hz). Compared with Fig. 9b, the contribution of high-speed, medium-speed and low-speed gears to 835Hz frequency component is relatively average in Fig. 11b. Medium-speed meshing frequency f_2 (417.6Hz) peak is more obvious, and the contribution is mainly high-speed stage, indicating the fault at high-speed stage. Fixed-axis gear box is connected with planetary gear box through medium-speed stage, and high-speed fault feature can only be transferred to planetary gear box through medium-speed stage, so medium-speed frequency amplitude increases on the transfer function.

In conclusion, it is found that the crack fault in root of high-speed gear

tooth increases high-speed axis rotation frequency of fixed axis gear box. The contribution of high-speed stage at this frequency is the largest, which is consistent with local fault characteristics of gear. High-speed fault characteristics are transmitted to planetary gear box to generate associated fault characteristics. Due to the limitation of signal transfer path, associated fault characteristic is mainly added to the frequency characteristic of connected part. In this paper, the associated fault characteristic is added to medium-speed meshing frequency. The contribution of associated fault characteristics can be traced back to the source to locate the location of fault. In this paper, the main contribution of associated fault characteristic f_2 (417.6Hz) is from high-speed stage, so it is determined that high-speed gear is faulty. From the transfer functions of fixed axis gearbox and planetary gearbox, it can be inferred that high-speed stage has fault.

5. Conclusion

In this study, the fault simulation test rig of wind turbine gear transmission system is taken as the research object. The three-dimensional solid rigid-flexible coupling model of system is established. According to the method of system identification, the transfer function model corresponding to each path is established. The signal transmission process is revealed through the transmission characteristic analysis, and the associated fault characteristics and fault transfer characteristics between gears under the crack fault state are obtained. It is found that the attenuation degree of signal is related to the distance between vibration source and measuring point. The farther the distance is, the greater the attenuation. Due to the limitation of signal transfer path, associated fault characteristic is mainly added to the frequency characteristic of connected part. The contribution of associated fault characteristics can be traced back to the source to locate the location of fault. The method of transfer function can be used to explore the source of unknown associated fault characteristics, which can provide theoretical basis for multi-gear fault diagnosis.

Acknowledgment

This research is supported by Baoji Science and Technology Plan Project (2017JH2-11).

REFERENCES

[1] *R. P. Shao, W. L. Guo, M. J. Liu*, "Analysis and simulation of dynamic in characteristic for cracked gear", Mechanical Science and Technology for Aerospace Engineering, **vol. 22**, no. 5, 2003, pp. 788-791.

[2] *Y. C. Zhang, R. P. Shao, H. Y. Liu*, "The influences of crack fault to dynamic characteristics in gear transmission system", Machinery Design&Manufacture, **vol. 10**, no. 10, 2006, pp. 12-14.

[3] *Z. G. Chen, Y. M. Shao*, "Dynamic simulation of planetary gear with tooth root crack in ring gear", Engineering Failure Analysis, **vol. 31**, no. 9, 2013, pp. 8-18.

[4] *X. H. Liang, M. J. Zuo, M. Pandey*, "Analytically evaluating the influence of crack on the mesh stiffness of a planetary gear set", Mechanism and Machine Theory, **vol. 76**, 2014, pp. 20-38.
[5] *W. Y. Liu, W. H. Zhang, J. G. Han, et al*, "A new wind turbine fault diagnosis method based on the local mean decomposition", Renewable Energy, **vol. 48**, no. 6, 2012, pp. 411-415.
[6] *Z. X. Li, X. P. Yan, Z. Tian, et al*, "Blind vibration component separation and nonlinear feature extraction applied to the non-stationary vibration signals for the gearbox muti-fault diagnosis", Measurement, **vol. 46**, 2013, pp. 259-271.
[7] *Z. X. Li, X. P. Yan, C. Yuan, et al*, "A fault diagnosis approach for gears using multidimensional features and intelligent classifier", Noise & Vibration Worldwide, **vol. 41**, no. 10, 2010, pp. 76-86.
[8] *Z. X. Li*, "A novel solution for the coupled faults isolation in gear pairs using the conception of frequency tracking", Elektronika Ir Elektrotechnika, **vol. 20**, no. 3, 2014, pp. 69-72.
[9] *C. Y. Luo, C. Q. Shen, W. Fan, et al*, "Research on the sparse representation for gearbox compound fault features using wavelet bases", Shock & Vibration, **vol. 2015**, no. 4, 2015, pp. 1-11.
[10] *Z. B. Zhang, Q. Wang, T. Gao*, "Study on Fault Diagnosis of Gearbox Based on FRF-Modified Method", Industrial Technology Innovation, **vol. 3**, no. 3, 2016, pp. 315-317.
[11] *L. B. Liu, X. H. Liang, M. J. Zuo*, "Vibration signal modeling of a planetary gear set with transmission path effect analysis", Measurement, **vol. 85**, 2016, pp. 20-31.
[12] *T. R. Pattabiraman, K. Srinivasan, K. Malarmohan*, "Assessment of sideband energy ratio technique in detection of wind turbine gear defects", Case Studies in Mechanical Systems and Signal Processing, **vol. 2**, 2015, pp. 1-11.
[13] *C. G. Cooley, R. G. Parker*, "The geometry and frequency content of planetary gear single-mode vibration", Mechanical Systems and Signal Processing, **vol. 40**, no. 1, 2013, pp. 91-104.
[14] *M. J. Zhang, Q. Cao*, Engineering mechanical dynamics, National Defense Industry Press, 2012.
[15] *B. W. Xu, Q. Y. Jiao*, Mechanical vibration and modal analysis basis, Mechanical Industry Press, 2014.
[16] *H. Zeng, Y. S. Wu, X. J. Wu, et al*, "The application of fault diagnosis of train bogie based on vibration energy and transfer function analysis", China Measurement & Test, **vol. 41**, no. 10, 2015, pp. 121-124.
[17] *X. G. Ma, W. Yang, X. M. You, et al*, "Multi-body dynamical analysis on rigid-flexible coupling for planetary gear system", Chinese Journal of Construction Machinery, **vol. 7**, no. 2, 2009, pp. 146-152.
[18] *Y. L. He, W. Huang, C. W. Li, et al*, "Flexible Multibody Dynamics Modeling and Simulation Analysis of Large-scale Wind Turbine Drivetrain", Chinese Journal of Mechanical Engineering, **vol. 50**, no. 1, 2014, pp. 61-69.
[19] *Z. G. Chen, Z. F. Zhu, Y. M. Shao*, "Fault feature analysis of planetary gear system with tooth root crack and flexible ring gear rim", Engineering Failure Analysis, 49, 2015, pp. 92-103.
[20] *Z. Chen, Y. Shao*, "Dynamic features of a planetary gear system with tooth crack under different sizes and inclination angles", Journal of Vibration and Acoustics, **vol. 135**, no. 3, 2013, 031004.
[21] *Y. Yang, Z. G. Chu, M. Xiong*, "Transfer path analysis of booming noise in a car cabin based on impedance matrix method", Journal of Vibration and Shock, **vol. 33**, no. 18, 2014, pp. 164-169+176.
[22] *R. Guo, S. Qiu, H. Q. Fang, et al*, "Advance in studying on transfer path analysis methods in frequency domain", Journal of Vibration and Shock, **vol. 32**, no. 13, 2013, pp. 49-55.